Prepared for submission to JINST

DIRC2017: Workshop on fast Cherenkov detectors
August 7-9, 2017
Castle Rauischholzhausen, Germany

Lifetime of MCP-PMTs and other Performance Features

A. Lehmann,[a,1] **M. Böhm,**[a] **W. Eyrich,**[a] **D. Miehling,**[a] **M. Pfaffinger,**[a] **S. Stelter,**[a] **F. Uhlig,**[a] **A. Ali,**[b] **A. Belias,**[b] **R. Dzhygadlo,**[b] **A. Gerhardt,**[b] **K. Götzen,**[b] **G. Kalicy,**[b] **M. Krebs,**[b] **D. Lehmann,**[b] **F. Nerling,**[b] **M. Patsyuk,**[b] **K. Peters,**[b] **G. Schepers,**[b] **L. Schmitt,**[b] **C. Schwarz,**[b] **J. Schwiening,**[b] **M. Traxler,**[b] **M. Düren,**[c] **E. Etzelmüller,**[c] **K. Föhl,**[c] **A. Hayrapetyan,**[c] **K. Kreutzfeld,**[c] **O. Merle,**[c] **J. Rieke,**[c] **M. Schmidt,**[c] **T. Wasem,**[c] **P. Achenbach,**[d] **M. Cardinali,**[d] **M. Hoek,**[d] **W. Lauth,**[d] **S. Schlimme,**[d] **C. Sfienti,**[d] **M. Thiel**[d]

[a] *Friedrich Alexander-University of Erlangen-Nuremberg, Erlangen, Germany*
[b] *GSI Helmholtzzentrum für Schwerionenforschung GmbH, Darmstadt, Germany*
[c] *II. Physikalisches Institut, Justus Liebig-University of Giessen, Giessen, Germany*
[d] *Institut für Kernphysik, Johannes Gutenberg-University of Mainz, Mainz, Germany*

E-mail: Albert.Lehmann@fau.de

Abstract: The $\overline{\text{P}}$ANDA experiment at FAIR will use DIRC detectors for the separation of hadrons. The compactness of the $\overline{\text{P}}$ANDA detector requires the image planes of these detectors to be placed inside the magnetic field of the solenoid. Due to this and other boundary conditions MCP-PMTs were identified as the only suitable photon sensors. Until recently the major obstacle for an application of MCP-PMTs in high rate experiments like $\overline{\text{P}}$ANDA were serious aging problems which led to damage at the photo-cathode and a fast declining quantum efficiency as the integrated anode charge (IAC) increased. With new countermeasures against the aging, in particular due to the application of an atomic layer deposition (ALD) technique to coat the MCP pores, the lifetime of MCP-PMTs has meanwhile increased by a factor >50 which is fully sufficient for $\overline{\text{P}}$ANDA. The recent results of our long-term lifetime measurements are discussed. New 2-inch MCP-PMT prototypes from Hamamatsu show an encouraging behavior. However, the currently best performing MCP-PMT is a 2-inch PHOTONIS tube with two ALD-layers which reaches an IAC of >16 C/cm^2 without any visible sign of aging. In the second part of these proceedings a new data acquisition system of the PADIWA/TRB type is presented which allows a quasi-parallel measurement of many MCP-PMT performance parameters. Especially unwanted effects like dark-count rate, crosstalk, ion after-pulsing, and recoil electrons can be studied in more detail than ever before. Exemplary results for these parameters are shown. The discussed DAQ system will be used for the comprehensive data quality checks of the MCP-PMTs being built into the DIRCs.

Keywords: Photon detectors for UV, visible and IR photons (vacuum), Microchannel-plate photomultipliers, Cherenkov detectors.

[1] Corresponding author.

Contents

1 Introduction

The $\overline{\text{P}}$ANDA experiment [1] at the new FAIR accelerator complex at GSI in Darmstadt, Germany, will study fundamental questions of QCD by measuring $\overline{p}p$ annihilation reactions at a very high rate of up to 20 MHz [2]. To reliably separate pions and kaons up to 4 GeV/c two novel Cherenkov detectors of the DIRC type [3] will be built. A "Barrel DIRC" (BD) will cylindrically surround the interaction region and an "Endcap Disc DIRC" (EDD) will cover the forward hemisphere [4–6]. Due to severe space limitations the focal plane of both detectors will reside inside a magnetic field of >1 Tesla. This requires low noise photon sensors with good position and excellent time resolution, capable of detecting single photons at a very high rate inside this B-field. It has been established that the only suitable sensors for this purpose are multi-anode microchannel-plate photomultipliers (MCP-PMTs).

2 Lifetime of MCP-PMTs

2.1 MCP aging and cure

Until recently a serious problem of MCP-PMTs was their aging effects. During the electron amplification process atoms and molecules in the residual gas get ionized. These ions may be accelerated towards the photo-cathode (PC) and hit it with a kinetic energy of ~1 keV. Over time the PC gets damaged and the quantum efficiency (QE) starts dropping. These aging effects are usually measured by investigating the QE as a function of the integrated anode charge (IAC). Prior to 2011 the best commercially available MCP-PMTs were left with only 50% of their original QE

after <200 mC/cm^2 [7, 8]. This was by far not enough for the $\overline{\text{P}}$ANDA DIRCs which over a period of 10 years are required to sustain an IAC of about 5 C/cm^2 at the BD and even more at the EDD.

Triggered by the needs of projects like Belle-2 [9], TORCH [10], and $\overline{\text{P}}$ANDA, several years ago the main manufacturers of MCP-PMTs (PHOTONIS, Hamamatsu, BINP) put more effort into the development of long-life MCP-PMTs. This included an improved vacuum quality inside the PMT, electron scrubbed surfaces of the MCPs, thin film layers in front of or between the MCPs [11], or the application of a more robust PC [12]. With these approaches a lifetime improvement of a factor 10 was reached [11, 13], but this was still not enough for $\overline{\text{P}}$ANDA. The main breakthrough against the aging of MCP-PMTs came with the application of an atomic layer deposition (ALD) technique [14–16] where the MCP pores are coated with an ultra-thin layer of Al_2O_3 or MgO. This layer prevents the MCP glass substrate from outgassing which significantly reduces the ion flux hitting the PC. Using this technique the IAC requirement of 5 C/cm^2 for the $\overline{\text{P}}$ANDA DIRCs was reached for the first time by a PHOTONIS XP85112 MCP-PMT with 10 µm pore size [17, 18].

2.2 Results with ALD-coated MCP-PMTs

Some years ago only very few lifetime measurements of MCP-PMTs were available, and moreover these were done in quite different environments and therefore difficult to compare. To allow a fair comparison of the different types of PMTs, we decided to set up an environment where the aging behavior of all available lifetime-enhanced MCP-PMTs can be measured in parallel [8, 17, 19]. The sensors are continuously illuminated with a common LED light source at 1 MHz rate with an intensity attenuated to the single photon level. This is comparable to $\overline{\text{P}}$ANDA DIRC conditions. The MCP pulse heights and the LED light intensity are permanently monitored, while QE, gain and dark-count rates (DCR) are measured at regular intervals. QE wavelength scans are done every few weeks and a QE surface scan at 372 nm is usually performed at intervals of several months. Currently a parallel illumination of up to sixteen 2-inch MCP-PMTs is possible in this setup. A homogeneously illuminated area of about 30 × 30 cm^2 at a distance of ~50 cm from a blue LED is accomplished with a Thorlabs square diffuser ED1-S50-MD. The ALD-coated MCP-PMTs that were or still are included in the setup are listed in table 1.

Table 1. Characteristics of the investigated prototype MCP-PMTs with ALD-coating. The numbers given in the row for the integrated anode charge (IAC) correspond to the different sensor IDs.

Manufacturer	PHOTONIS	Hamamatsu		
Type	XP85112	R10754X-M16M	R13266-M64	R13266-M768
Sensor ID	1223 / 1332 / 1393	KT0001 / 0002	JS0022 / 0035	JS0018 / 0027
Pore size (µm)	10	10	10	
Pixels	8×8	4×4	8×8	8×128
A_{active} (mm^2)	53×53	22×22	51×51	
A_{total} (mm^2)	59×59	27.5×27.5	61×61	
Geom. eff. (%)	81	61	70	
IAC (C/cm^2)	9.23 / 15.91 / 16.25	18.90 / 17.32	4.23 / 3.57	0.97 / 1.98
Comments	ALD-surfaces; 1- / 1- / 2-layer	ALD and film btw. 1^{st} & 2^{nd} MCP	ALD and film in front of 1^{st} MCP	

Gain, DCR and relative QE (normalized to 350 nm for each IAC point) for various wavelengths as a function of the IAC are compared in figure 1 for different types of MCP-PMTs: a PHOTONIS XP85112 (9001332) with one ALD-layer, a PHOTONIS XP85112 (9001393) with two ALD-layers, a 1-inch Hamamatsu R10754X (KT0001) with one ALD-layer and a film between the first and second MCP, and a 2-inch Hamamatsu R13266 (JS0035) with one ALD-layer and a film in front of the first MCP. We observe the following behavior: there are some gain fluctuations but with increasing IAC no clear trends are visible; once the aging process starts, as seen in the relative QE, the DCR is declining rapidly; the MCP-PMTs 9001332 and the KT0001 show a wavelength dependent QE after 10 and 5 C/cm^2, respectively, while the 9001393 and the JS0035 show no aging effects until >16 C/cm^2 and the 3.5 C/cm^2 acquired to date, respectively. Although the faster dropping QE for long wavelengths and the declining DCR seem to be a clear aging sign, whilst a plausible reason might be a change in the PC work function, this explanation is too simple as was discussed in ref. [20]. Currently it is not clear which mechanisms are responsible for the PC aging of MCP-PMTs.

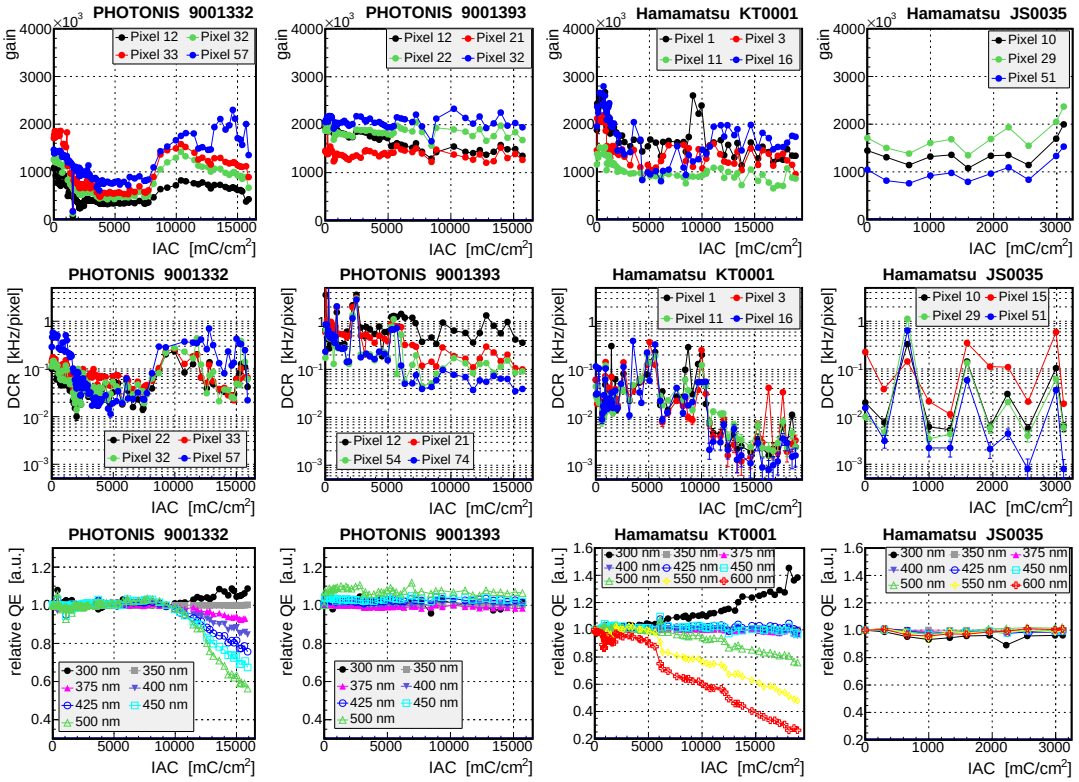

Figure 1. Gain [upper], DCR [middle] and relative QE with the other wavelengths normalized to 350 nm [lower] as a function of the IAC. Compared are ALD-coated MCP-PMTs (columns from the left): PHOTONIS XP85112 9001332, 9001393, and Hamamatsu R10754X-M16M KT0001, R13266-M64 JS0035.

The results of QE surface scans at 372 nm are shown in figure 2 for the four MCP-PMTs discussed in the previous paragraph. While the QE starts dropping for the PHOTONIS 9001332 on the unmasked left side at >10 C/cm^2 IAC, the 9001393 with two ALD-layers shows no sign of QE damage even after ~15 C/cm^2. It is yet unclear why the QE of the 9001332 also starts dropping

at the masked right half after ~13 C/cm^2. A possible explanation could be neutral residual gas reacting at the PC surface as was suggested in ref. [11]. The behavior is not seen in the PHOTONIS 9001223 [21]. The QE of the Hamamatsu JS0035 is still unaffected after moderate ~2.5 C/cm^2 IAC, whereas the QE of the KT0001 is declining after >5 C/cm^2 IAC with clearly more damage in the corners. This pronounced aging near the rims and corners was observed before [18], but no explanation of this effect can be given to date. A speculative argument could be that some sealing material of the MCP-PMT spoils the surface near the PC rims.

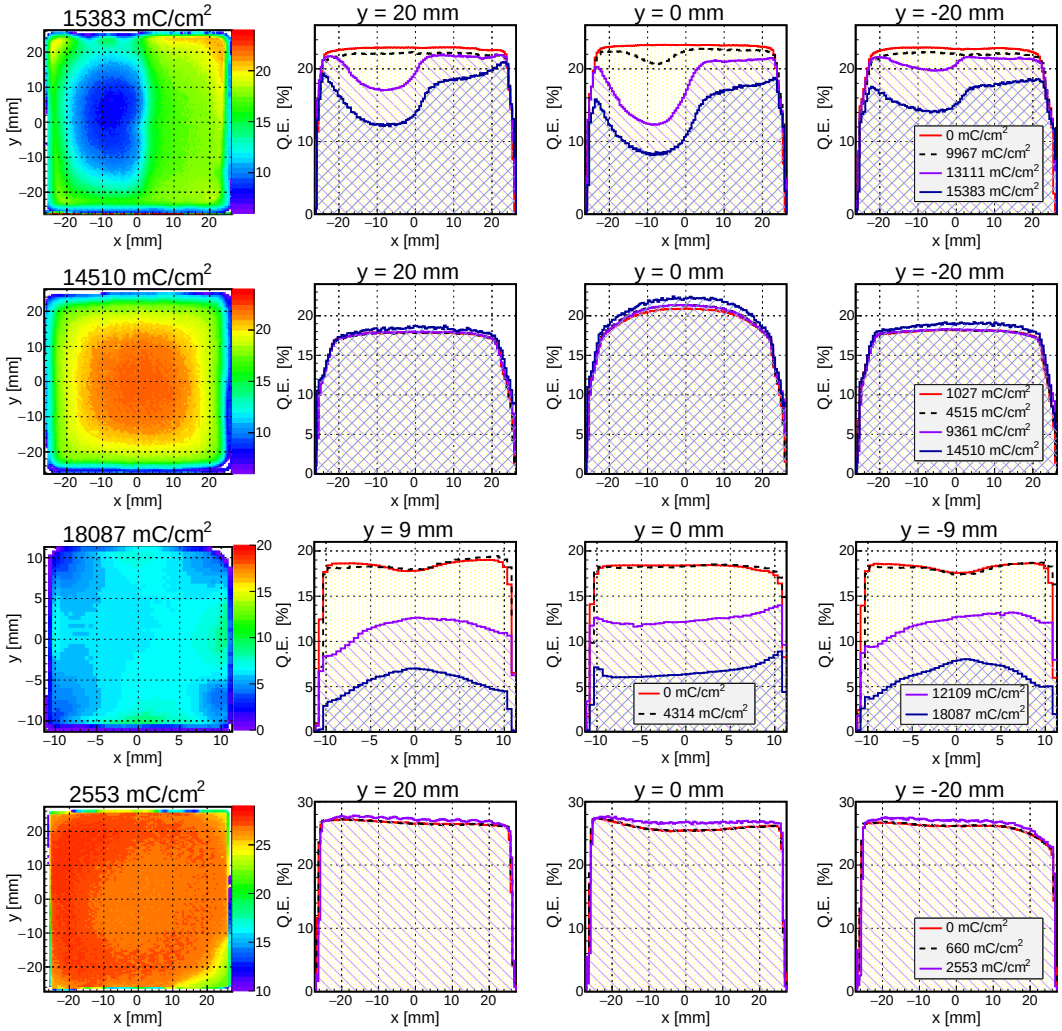

Figure 2. QE at 372 nm as a function of the PC surface for some ALD-coated MCP-PMTs. 1st row: PHOTONIS XP85112 9001332 (right PC half masked); 2nd row: PHOTONIS 9001393 (unmasked); 3rd row: Hamamatsu R10754X-M16M KT0001; 4th row: Hamamatsu R13266-M64 JS0035. Left column: 2d QE charts (in % [color level]); other columns: QE x-projections at different y-positions and anode charges.

A compilation of the QE dependence at 400 nm as a function of the IAC is compared in figure 3 for all investigated MCP-PMTs with ALD-coating. The data for a Hamamatsu R10754 with only a protection film in front of the first MCP, but no ALD-coating yet, is shown for comparison (blue dots). The breakthrough in the lifetime of MCP-PMTs was obviously reached with an application

of the ALD-technique. All measured tubes from PHOTONIS and Hamamatsu (1-inch) exceed the $\overline{\text{P}}$ANDA lifetime benchmark of 5 C/cm^2 IAC, some even significantly so. However, there is a difference in the aging behavior: the QE of the PHOTONIS 9001223 and 9001332 with one ALD-layer is very stable up to a certain IAC (6 and 10 C/cm^2, respectively) and starts continuously degrading thereafter. The QE of the 1-inch Hamamatsu KT0001 and KT0002 is slowly but steadily dropping until ~14 C/cm^2 when the QE gets lower than 50% of its original value. The first 2-inch prototypes from Hamamatsu (JS0018 and JS0022) had poor IAC behavior while the later MCP-PMTs of this type behave better. For these tubes a final evaluation has to wait until the benchmark of 5 C/cm^2 IAC has been reached. Nevertheless, a clear improvement is seen in the later 2-inch prototypes from Hamamatsu. The best performing MCP-PMT by far is the PHOTONIS 9001393 with two ALD-layers where no sign of aging is visible at an IAC of >16 C/cm^2. This is an improvement by a factor of ~10 compared to lifetime optimization techniques other than ALD and a factor of almost 100 compared to pre-lifetime-enhanced MCP-PMTs. Similar results were obtained by MCP-PMT lifetime measurements for the Belle-2 experiment [22].

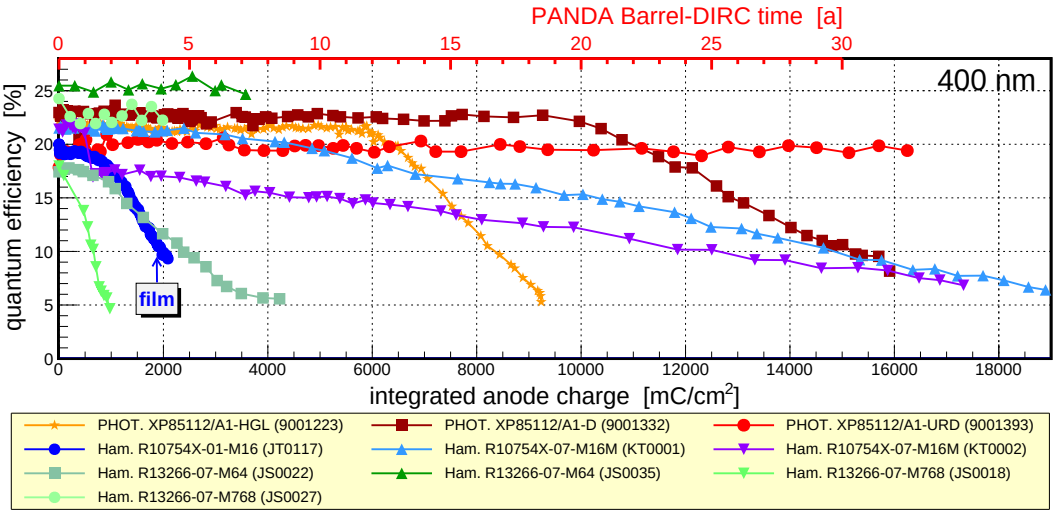

Figure 3. Comparison of the lifetime results for different ALD-coated MCP-PMTs: QE as a function of the integrated anode charge (IAC) at 400 nm. A 1-inch Hamamatsu MCP-PMT (blue dots) with no ALD-layers, but a protection film in front of the first MCP is shown for comparison. The upper x-axis illustrates the PANDA lifetime in years assuming plausible run parameters [23]

3 Other Performance Features

3.1 Measurement setup

Besides the typical performance parameters of gain, time resolution, overall DCR, rate capability, and lifetime of multi-anode MCP-PMTs there are less easily measurable parameters as DCR per anode pad, after-pulsing triggered by feedback ions, spacial and temporal electron recoil distributions off the MCP input, and crosstalk (charge-sharing and electronic) between all anode pads. For a more detailed explanation of the latter parameters see the subsections 3.2 to 3.5. With the setup of a new data acquisition system we are able to study these parameters in detail.

The PC of an MCP-PMT is illuminated with a fast ($\sigma_t \approx 15$ ps) blue or red laser where the light intensity is reduced to single photon level by neutral density filters and the light spot is focused to ~50 µm peak width. The MCP-PMT's anode signals are 10x amplified and fed into a FPGA-based 16 channel PADIWA1 (PANDA DIRC WASA) discriminator board [24]. The timing signals are then processed by the multihit TDCs of the FPGA-based HADES TRB3 (Trigger and Readout Board version 3) [24, 25] which additionally delivers coarse pulse height information by applying a time-over-threshold (ToT) technique. These DAQ boards have a flexible design and provide a time precision down to ~10 ps per single TDC channel. Each channel can store the time information of up to 127 hits per trigger and digest burst hit rates of up to 66 MHz. This TRB/PADIWA system permanently analyzes the data stream delivered by all anode pads of an MCP-PMT. The lead time (= timing of the pulse leading edge) and the ToT information of each hit and TDC channel (corresponding to an anode pad) are continuously queued in a ring buffer and can be read out and stored within an adjustable time interval (e.g., -10 to +10 µs) around a given trigger time which in the presented analysis is artificially shifted to t_0 = 100 ns for each channel. In our case this is usually the trigger pulse of a PiLas laser.

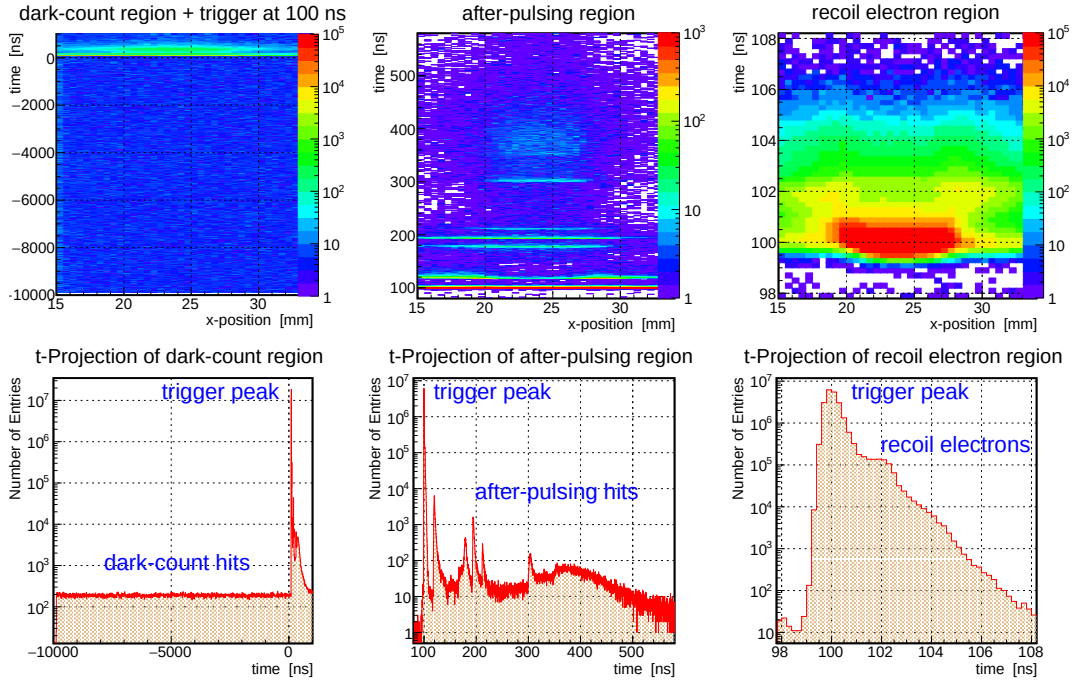

Figure 4. Information obtainable with TRB/PADIWA scans for the PHOTONIS XP85012 (9002085) HiQE MCP-PMT. Left: 2d-distribution (upper) and its time projection (lower) of the laser x-position versus the lead time for hits registered in the arbitrary anode pixel x4-y6. The time window from -10 to +1 µs contains all hits of interest, in particular the dark-count region from -10 to 0 µs. The trigger peak at 100 ns corresponds to photons from the laser pulse. Center: same as for the left plots, but zoomed to a time window from 80 to 580 ns containing the trigger peak and the after-pulse hits at t_0 > 100 ns. Right: further zoomed to a time window from 98 to 108 ns containing the trigger peak, the hits from recoil electrons (little later than 100 ns), and events where the charge cloud is distributed across adjacent anode pads (charge-sharing takes place around 100 ns but at x-positions left (x < 20 mm) and right (x > 27 mm) of the read out anode pixel x4-y6 which stretches from x ≈ 20 to 27 mm (compare also to the left plot in figure 7).

By running an xy-scan (in steps of 0.5 or 1.0 mm) across the active surface of the MCP-PMT the information x-, y-position of the laser spot, lead time, ToT, and number of hits, are obtained and stored to disk for each anode pad (channel) and laser pulse. From this raw information we can deduce the previously mentioned dark-count xy-distributions, the after-pulsing distributions as a function of the xy-position and of the time after the trigger pulse (quasi the TOF of the feedback ions), and the recoil electron distributions in space and time. Counting the hits within narrow and wide time windows the charge-sharing and electronic crosstalk behavior can be analyzed. Thus with these TRB scans the separation of charge-sharing events from those of recoil electrons and after-pulsing hits becomes possible.

X-position versus time distributions at different time windows of a new HiQE PHOTONIS XP85012 (9002085) MCP-PMT are plotted in figure 4. In these distributions the number of hits measured in the exemplary anode pad x4-y6 are plotted for laser x-positions between 15 and 34 mm covering also the left and right adjacent anode pads. In the left plots a wide time window from -10 and +1 µs is plotted from which we deduced the DCR by integrating the number of hits between -10 and 0 µs before the trigger (at 100 ns). The center plots show a zoomed time window from 80 to 580 ns which contains the after-pulse events arriving later than the trigger pulse at 100 ns. In the right plots the time window is zoomed to very close around the main trigger peak which contains the recoil electron and charge-sharing events. The overall time resolution is of the order of 150-200 ps. This is worse than anticipated and the reason is still under investigation.

3.2 Dark-count map

A by-product of the previously described scans is a dark-count map for all anode pixels of each investigated MCP-PMT. The DCR, caused by thermal electron emission from the PC, for an anode pixel is deduced from the number of hits in the time interval from -10 to 0 µs before the actual trigger peak and is then scaled by 10^5 to get the DCR in Hz. At a typical laser trigger rate of <10 kHz this time window is free of other background hits like after-pulses and recoil electrons. In the plots (left column) of figure 4, it is clearly seen that the DCR distribution is uniform within this time window, as expected. The measured DCR/pixel for three 8×8 pixel MCP-PMTs are shown in figure 5, which vary between <10 Hz and ~10 kHz. We also observe that pixels with high DCR are usually found at the edges or corners and not in the center of the anode region. This is the case for most scanned MCP-PMTs but the reason for the effect is currently unknown. The lowest integral DCR of ~500 Hz was observed for the Hamamatsu JS0035, the highest of ~60 kHz for the PHOTONIS 9001393. This is consistent with the levels of DCR shown in figure 1.

3.3 After-pulsing

The new TRB/PADIWA data acquisition system allows the identification and quantification of after-pulse events. These events are caused by feedback ions of the residual gas hitting the PC and releasing an electron which is then also amplified in the MCPs but arriving later than the electrons of the main trigger. As seen in figure 4 the times of after-pulse hits range from the trigger peak at 100 ns to about 1 µs. In figure 6 the after-pulse TOF distributions of three different MCP-PMTs are compared. The TOF peaks in these plots correspond to heavy (e.g., Cs and Pb) and light (e.g., H, He, ...) residual gas ions most likely produced in the first MCP layer. The broad continua underneath these peaks are probably caused by ions which are scattered inside the MCP pores with the latest

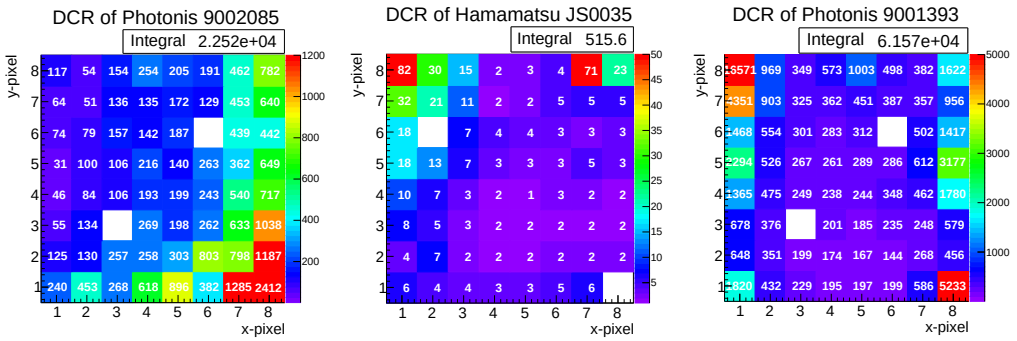

Figure 5. DCR xy-maps per anode pad for the 2-inch MCP-PMTs PHOTONIS XP85012 (9002085, non-ALD), PHOTONIS XP85112 (9001393, two ALD-layers), and Hamamatsu R13266 (JS0035, ALD+film). The average gain of the MCP-PMTs is set to $\sim 10^6$ and the threshold is well below the typical single photon pulse height. The white pads are caused by dead channels in the PADIWA frontend boards. The color-coded scale (z-axis) corresponds to DCR/pixel in Hz.

broad hit accumulation stemming from ions produced in the second MCP. The overall structure of the after-pulse TOF distribution of an individual MCP-PMT is often difficult to interpret. However, it is possible to quantify the after-pulse rate for each MCP-PMT. For this we calculate the ratio of hits within the time interval from 115 to 550 ns to hits within the trigger window from 98 to 115 ns. This provides the fraction of after-pulse hits, in principle per anode pixel. From the fractions given in figure 6 we see that there is no big difference between aged ALD-coated and new non-ALD MCP-PMTs. Surprising is the relatively high after-pulse fraction for the Hamamatsu MCP-PMT with ALD-coating and a film in front of the first MCP, where one expects a very low after-pulse fraction because the film should prevent the ions from reaching the PC. This could point to an imperfect sealing of the input MCP surface. From quality assurance measurements over a large sample of MCP-PMTs we expect a better picture of the after-pulsing behavior which might help in designing new MCP-PMTs with even less feedback ions.

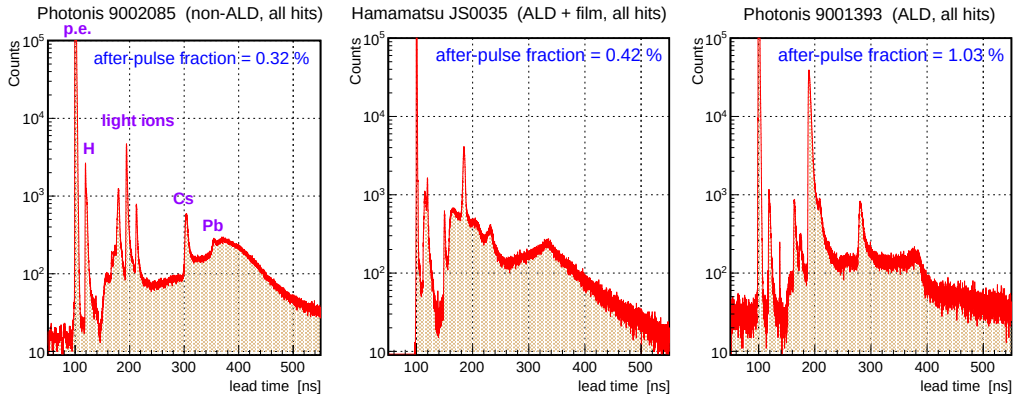

Figure 6. After-pulse time-of-flight (TOF) spectra (from left to right) for the 2-inch MCP-PMTs PHOTONIS XP85012 (9002085, non-ALD), Hamamatsu R13266 (JS0035, ALD-coated + film), and PHOTONIS XP85112 (9001393, 2 ALD-layers). The trigger peak at 100 ns corresponds to direct photo electrons (p.e.). Some of the other peaks can be assigned to feedback ions from the residual gas, as indicated in the left plot.

3.4 Recoil electrons

In the time region closely after the trigger peak at 100 ns a clear structure is visible in the right plots of figure 4, whose number of entries decreases over several orders of magnitude up to ~8 ns. These hits are caused by electrons which recoil from the input surface of the first MCP layer and cause a later and spatially shifted avalanche when the scattered electron reaches an MCP pore in a second or later step. In the 2d-information x-position versus time of figure 7 (left), this structure can be identified as occurring close to the read out anode pixel. The xy spatial distribution of these hits can be studied by moving the time window. In the plots (center and right) of figure 7 one observes that with a narrow time cut around the trigger peak, only the region of the read out anode pixel x3-y6 is populated, while at later times this pixel is also hit when the laser focus points to the vicinity of the pixel position. The spatial and temporal extension of ~8 mm and ~2 ns of these events fit well the expectations for recoil electrons which are backscattered from the MCP input before they are amplified. The events at later times could be caused by electrons that are scattered more than once.

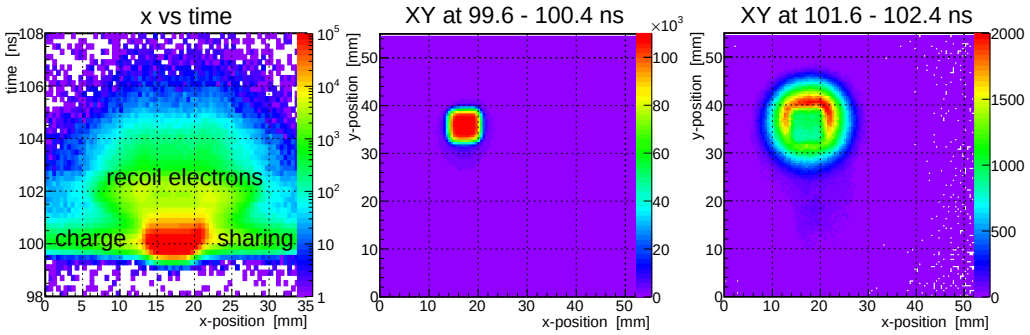

Figure 7. Temporal and spatial distribution of recoil electrons for the PHOTONIS XP85012 (9002085). Left: distribution x-position versus time when the pixel x3-y6 registered a hit, the population regions expected for recoil electrons and charge-sharing events are labelled; center: xy hit distribution for hits very close (99.6 to 100.4 ns) around the trigger peak from direct electrons; right: xy distribution for timely shifted hits (101.6 to 102.4 ns) corresponding to recoil electrons.

3.5 Crosstalk

By counting the number of hit anode pixels within a narrow time window around the trigger peak at 100 ns the charge-sharing crosstalk can be studied. When the charge cloud reaching the anode plane is distributed across two or more anode pads these hits will arrive simultaneously in time. In figure 8 (left) we see the 8×8 pixel structure if only one hit is measured. For two hits at the same time (center) we observe a population of the pixel borders and with >2 hits (right) mainly the pixel corners are visible. Analyzing the widths of these charge-sharing cross talk events we are able to estimate the size of the charge cloud of 1.0 to 1.2 mm (σ) for this MCP-PMT. We would like to note here that for the new Hamamatsu 2-inch tube R13266 the charge-sharing cross talk is much lower, in the presented type of analysis it is basically invisible. This is probably due to the fact that the distance between the MCP output and the anode plane is considerably shorter than in the PHOTONIS devices. In principle the TRB scans will also allow the quantification of electronic crosstalk effects. Since this analysis is still ongoing, we cannot show any results in this paper yet.

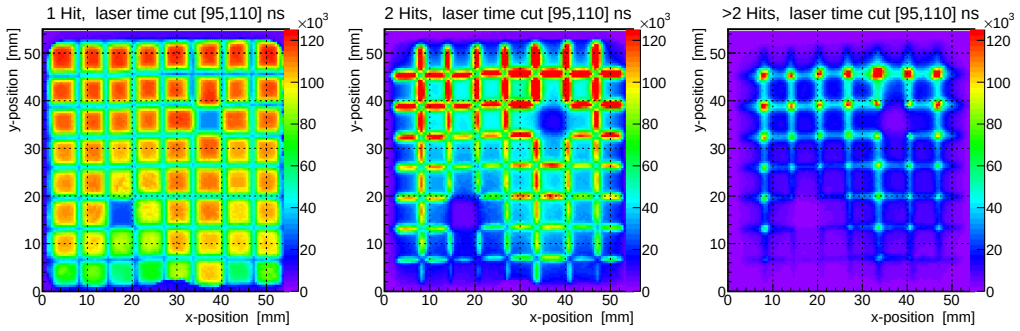

Figure 8. Charge-sharing crosstalk reflected in xy-distribution for hits within 15 ns of the laser trigger for PHOTONIS XP85112 (9002085): left: 1 anode hit; middle: 2 anode hits; right: ≥2 anode hits. The two holes correspond to dead PADIWA channels.

4 Conclusions

In our aging measurements of MCP-PMTs over the last seven years we have seen a tremendous increase of the lifetime by a factor of almost 100. This was realized by applying an ALD-technique where the MCP pores are coated with an ultra-thin atomic layer to lower or even prevent outgassing of atoms desorbed in the MCP glass substrate. In this way the ion bombardment of the PC is reduced and less damage takes place. Except for the 2-inch Hamamatsu prototypes, all measured MCP-PMTs with ALD-coating reach the minimum requirement of 5 C/cm^2 integrated anode charge for the $\overline{\text{P}}$ANDA DIRC detectors. With this result the realization of these detectors is secured.

The new TRB/PADIWA data acquisition system allows the realization of an efficient quality assurance program for the MCP-PMTs of the $\overline{\text{P}}$ANDA DIRCs. In addition to the performance parameters of gain, time resolution and rate capability, this system will allow the investigation and quantification of background parameters such as dark-count rate, ion after-pulsing, distribution of recoil electrons, and in particular crosstalk among the anode pixels. The results presented in this paper are encouraging and may open a new window in studying the performance and characteristics of MCP-PMTs.

Acknowledgments

We thank our Erlangen colleagues from ECAP for granting use of the QE setup. The companies PHOTONIS and Hamamatsu we thank for helpful conversations. This work is supported by the German BMBF and GSI Darmstadt.

References

[1] PANDA Collaboration, *Technical Progress Report*, FAIR-ESAC/Pbar 2005

[2] PANDA Collaboration, *Physics Performance Report*, 2009, [hep-ex/arXiv 0903.3905v1]

[3] P. Coyle et al., *The DIRC counter: a new type of particle identification device for B factories*, Nucl. Instr. Meth. **A 343** (1994) 292

[4] C. Schwarz et al., *The PANDA DIRC detectors at FAIR*, 2017 *JINST* **12** C07006

[5] R. Dzhygadlo et al., *The PANDA barrel DIRC*, 2016 *JINST* **11** C05013

[6] M. Düren et al., *The Endcap Disc DIRC of PANDA*, Nucl. Instr. Meth. **A 876** (2017) 198

[7] N. Kishimoto et al., *Lifetime of MCP-PMT*, Nucl. Instr. Meth. **A 564** (2006) 204

[8] A. Britting et al., *Lifetime-issues of MCP-PMTs*, 2011 *JINST* **6** C10001

[9] K. Inami, *TOP counter prototype R&D*, Nucl. Instr. Meth. **A 639** (2011) 298

[10] T. Gys et al., *The TORCH detector R&D: Status and perspectives*, Nucl. Instr. Meth. **A 876** (2017) 156

[11] T. Jinno et al., *Lifetime-extended MCP-PMT*, Nucl. Instr. Meth. **A 629** (2011) 111

[12] M. Yu. Barnyakov and A. V. Mironov, *Photocathode aging in MCP PMT*, 2011 *JINST* **6** C12026

[13] A. Lehmann et al., *Significantly improved lifetime of microchannel-plate PMTs*, Nucl. Instr. Meth. **A 718** (2013) 535

[14] D.R. Beaulieu et al., *Nano-engineered ultra-high-gain microchannel plates*, Nucl. Instr. Meth. **A 607** (2009) 81

[15] M. Wettstein et al., *Development of sub-nanosecond, high gain structures for time-of-flight ring imaging in large area detectors*, Nucl. Instr. Meth. **A 639** (2011) 148

[16] O.H.W. Siegmund et al., *Atomic layer deposited borosilicate glass microchannel plates for large area event counting detectors*, Nucl. Instr. Meth. **A 695** (2012) 168

[17] A. Lehmann et al., *Lifetime of MCP-PMTs*, 2014 *JINST* **9** C02009

[18] A. Lehmann et al., *Improved lifetime of microchannel-plate PMTs*, Nucl. Instr. Meth. **A 766** (2014) 138

[19] A. Lehmann et al., *Systematic studies of micro-channel plate PMTs*, Nucl. Instr. Meth. **A 639** (2011) 144

[20] A. Lehmann et al., *Recent developments with microchannel-plate PMTs*, Nucl. Instr. Meth. **A 876** (2017) 42

[21] A. Lehmann et al., *Tremendously increased lifetime of MCP-PMTs*, Nucl. Instr. Meth. **A 845** (2017) 570

[22] K. Matsuoka et al., *Extension of the MCP-PMT lifetime*, https://doi.org/10.1016/j.nima.2017.02.010

[23] A. Lehmann et al., *Lifetime of MCP-PMTs*, 2016 *JINST* **11** C05009

[24] A. Neiser et al., *TRB3: a 264 channel high precision TDC platform and its applications*, 2013 *JINST* **8** C12043

[25] C. Uğur et al., *A 16 channel high resolution (<11 ps RMS) Time-to-Digital Converter in a Field Programmable Gate Array*, 2012 *JINST* **7** C02004